Fractals, Vol. 10, No. 3 (2002) 00–00

MULTIFRACTAL CHARACTERIZATION OF REMOTELY SENSED VOLCANIC FEATURES: A CASE STUDY FROM KILAUEA VOLCANO, HAWAII

DANY C. HARVEY,* HÉLÈNE GAONAC'H,† SHAUN LOVEJOY‡ and JOHN STIX§
Département de Géologie, Université de Montréal
C.P. 6128, succ. Centre-ville
Montréal, Québec, Canada, H3C 3J7
**harveyda@thermos.geotop.uqam.ca*
†*GEOTOP, Université du Québec à Montréal*
C.P. 8888, succ. Centre-ville
Montréal, Québec, Canada, H3C 3P8
helene@thermos.geotop.uqam.ca
‡*Department of Physics, McGill University, Montreal*
Québec, Canada, H3A 2T8
lovejoy@physics.mcgill.ca
§*Earth and Planetary Sciences, McGiff University*
Montreal Quebec, Canada
stix@eps.mcgilloca

DANIEL SCHERTZER
Laboratoire de Modélisation en Mécanique, Case 162
Université P. et M. Curie, 4
place Jussieu, Paris cedex 05, France
schertze@ccr.jussieu.fr

Abstract

We used a multifractal approach to characterize scale by scale, the remotely sensed visible and thermal-infrared volcanic field, at Kilauea Volcano, Hawaii, USA. Our results show that (1) the observed fields exhibit a scaling behavior over a resolution range of ∼2.5 m to 6 km, (2) they show a strong multifractality, (3) the multifractal parameters α, C_1 and H are sensitive to volcanic structural classes such as vent cones, lava ponds and active to inactive lava flows,

(4) vegetation area and volcanic gas plumes have a strong effect on the multifractal estimates, and (5) vegetation- and clouds-free images show statistical characteristics due to topography-related albedo in the visible and predominantly solar heating in the thermal infrared wavelengths.

Keywords: Multifractals; Volcanoes; Remote Sensing; Scaling; Fractals; Infrared.

1. INTRODUCTION

Due to its safe, synoptic viewing of rapid volcanic changes, remote sensing is particularly appropriate for monitoring active volcanic environments. While volcanoes have been observed in very different parts of the electromagnetic spectrum, not very many studies have been performed to quantitatively characterize the spatial distribution of the corresponding radiative fields. In particular, the highly variable aspect of volcanic thermal fields has been largely ignored. As an example, in volcanology, temperature gradients from Landsat TM rarely exceed 10°K/120 m while variations from *in situ* thermocouple measurements can readily exceed 200°K/m.[1,2] By smoothing or truncating this variability, many authors have proposed simplistic geophysical models.

However, in recent years a few authors have attempted to take into account the subpixel variability of such fields. For example, at low resolutions, Rothery et al.[3] suggested the "dual-band method" to estimate subpixel temperatures of either crust or hot lava as well as their spatial distributions. On the other hand, other authors[4,5] have proposed a new approach assuming large subpixel heterogeneity to characterize such highly variable fields based on the scaling properties of the observed fields at different scales, such as the volcanic albedo and the thermal field of volcanic features. Indeed, there is growing evidence that the variability shows scaling symmetries. These symmetries are typically expressed by power laws involving exponents which characterize the statistical behavior of a field over a wide range of spatial scales. For example, a classical power law function characterizes the area of a lava flow as a function of the resolution.[4] In this simple example, a geometric fractal set defines the lava covered regions and the scaling exponent is a fractal dimension. However, most geophysical phenomena are best represented as mathematical fields (not geometric sets) and they are associated with a hierarchy of fractal sets and dimensions: multiscaling behavior requires multifractal approaches.[6] This hierarchy may be expressed by a scaling exponent function which characterizes the field in an observer- (resolution) independent way. It has been demonstrated that various geophysical fields may show extreme but scaling spatial/temporal variability over a wide range of scales, e.g. recent works concerning various surface fields,[7–12] atmospheric temperature fields.[13,14] This variability can result from nonlinear dynamics repeating scale after scale, building up highly variable, often large intensities with fractal structures over a wide range of scales.

In the present paper, we characterize the nonlinear spatial distribution of the volcanic radiance over a wide range of scales by examining the scaling and estimating statistical multifractal parameters occurring on the Kilauea Volcano at Hawaii using visible and thermal infrared wavelengths to better constrain the spatial distribution of volcanic and non-volcanic features present in the area. We then compare the results with other geophysical fields, and finally we consider the implications for volcanology.

2. DATA SET

The current activity on Kilauea is located along an important fracture called the East Rift Zone on the eastern flank of the volcano shield since 1983. The activity successively built up a 255 meter elevation lava/spatter cone at Puu Oo as well as an active lava pond at Kupaianaha associated with lava tubes flowing down to the ocean. In order to study this, the Jet Propulsion Laboratory has carried out a variety of NASA-sponsored airborne remote sensing observations over the Puu Oo and Kupaianaha vents between 1985 to 1991. Selected images used here cover three periods of volcanic activity during the period of November 1985 to October 1988. Data were collected from NASA C-130B aircraft using the NS001 multispectral scanner which collects

data over eight channels in the visible, short and long wavelengths infrared regions of the spectrum. The October 1988 campaign included a useful night-time flight to study the effect of the diurnal variation and the increased thermal contrast between active and non-active volcanic regions. The data were collected with an 8-bit dynamic range which leads to a complete grayscale of 0 (black) to 255 (white) digital number (DN) values.

The component of the surface (bidirectional) reflectance, which is measured by the visible channels, depends on the intrinsic (microscopic) absorption/reflection properties of the surface as well as the surface element orientation (e.g. roughness). In contrast, the thermal infrared (TIR) images originate in black body emission, hence are dependent on both temperature and emissivity. In both cases, the sensor resolution is far lower than the homogeneity scale so that nontrivial, nonlinear averaging effects are involved. Differences in the thermal radiance can therefore be produced either by temperature variations at the source or by differences in emission properties of the material.

We selected sub-scenes of images acquired in two of the eight NS001 instrument spectral bands (band #2; 0.529–0.603 μm and band #8; 10.9–12.3 μm). Each 2D sub-scene has either a 512×512 or 256×256 pixel size and is centered on active volcanic features observed at Kilauea: (1) the Puu Oo volcanic cone and surroundings, (2) the Kupaianaha lava pond and surroundings, and (3) a section of the lava field which encompasses an active lava tube (Fig. 1). In the first two cases, the activity follows quasi-radial fracture networks via degassing whereas in the latter, it represents a hot, thermal emitting roofed lava tube channeling through a cooling lava flow field.

Variations in aircraft height above the ground result in ground resolutions varying from one sub-scene to another from 2.9 m/pixel to 12.9 m/pixel. In the visible, the structure of lava flow field surfaces and localized volcanic gas plumes are the dominant volcanic features. Large thermal anomalies related to volcanic activity are extremely sparse, and when they occur, occupied less than five to ten pixels in size (see below). Gas plumes often saturate the sensor, but the saturation represents in the worst case only 8% of the total area (although unfortunately, they are concentrated in the interesting hot spots). The contrast between the vegetation area and surrounding lava flows is quite low. In thermal-infrared (TIR), volcanic gas plumes and atmospheric clouds occur at very low emission and contrast poorly with the background. Obviously, active areas present highly intense spikes with $DN > 200$. In daytime sub-scenes, older inactive flows show moderate to high intensities due to their emissive properties while vegetation is represented by very low intensities. In night-time images, these DN-values decrease slightly. However, several sub-scenes show pixel saturation associated with high temperature events. This is a consequence of the relatively narrow dynamic range of the sensor (8-bit).

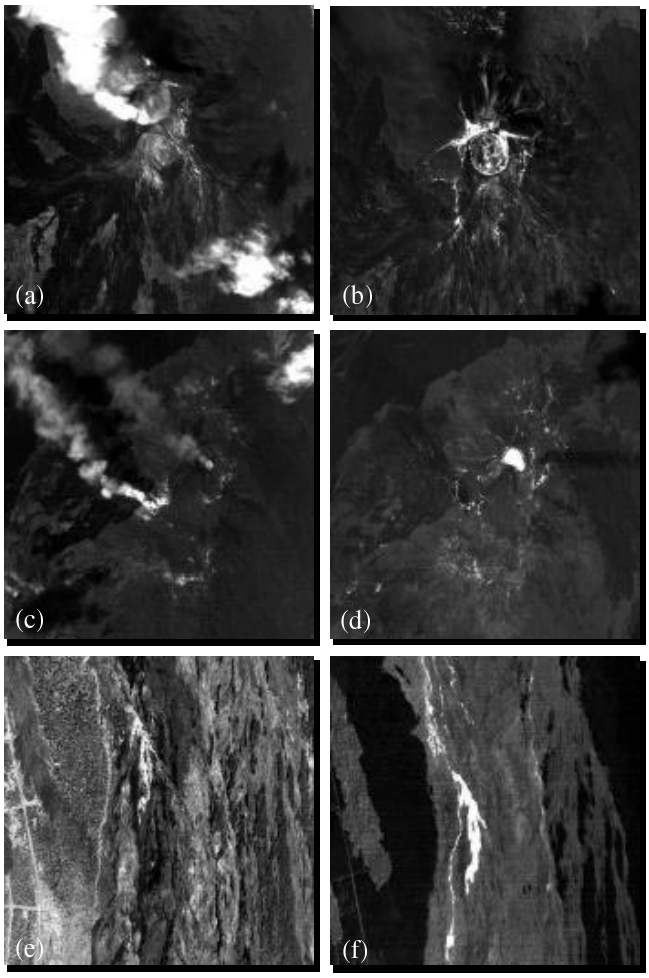

Fig. 1 Example of classes of volcanic structures analyzed. In **(a)**, the Puu Oo volcanic cone from the visible (band 2) and **(b)** from the thermal infrared (band 8) of NS001. In **(c)**, the Kupaianaha lava pond from the visible and **(d)** from the thermal infrared. In **(e)**, an active lava flow and associated lava tube from the visible and **(f)** from the thermal infrared. The lava breakout occurring in **(e)** and **(f)** was only present on few image data, otherwise only the narrow lava tube and some small skylights showed high thermal anomalies.

3. PRESENCE OF SCALING AND MULTISCALING

We first exhibit the scaling of the data. The energy spectrum analysis is a sensitive indicator of scaling and its limits.[5,7,15–17] The isotropic energy spectrum $E(k)$ is the squared modulus of the ensemble averaged, angle integrated Fourier transform. When the field of interest exhibits isotropic scale invariant properties, we can write:

$$E(k) = k^{-\beta} \tag{1}$$

where β is the invariant scaling exponent and k the spatial wavenumber (cycles/m).

Figure 2 shows that the scaling behavior is observed over essentially all the observed range of scales, i.e. from 2.5 m to 6200 m for all analyzed subscenes with no significant break in individual samples. For all volcanic features in each spectral band, as well as from one band to another, the results give β-values ranging from 0.8–2.0. Although we observed slight anisotropies due to preferential directions of some volcanic structures, the anisotropy is largely washed out by the angle integration of the spectral density and does not seem to globally affect the Fourier exponents of the data greatly. Since the anisotropy itself is likely to be scaling, more studies are currently being done on this aspect.

Multiplicative cascade models were first developed to model the variability of conservative fields in turbulence.[18–20] Going from the scale ratio $\lambda = 1$ to $\lambda = \Lambda = L/\ell_0$ (large outer scale L to smallest scale ℓ_0), the probability distribution of the intensities can be described by:

$$\Pr(\varepsilon_\lambda \geq \lambda^\gamma) \approx \lambda^{-c(\gamma)} \tag{2}$$

$$\varepsilon_\lambda \approx \lambda^\gamma \tag{3}$$

where γ is the singularity order (related to the intensity or DN value at one pixel), $c(\gamma)$ is the associated codimension function, and ε_λ is the pixel intensity at a scale ratio λ of the field. It is convenient (and equivalent) to consider the qth order (ensemble averaged) statistical moments. If Eq. (2) holds, then the following is the corresponding expression for the scaling of the moments:

$$\langle \varepsilon_\lambda^q \rangle \propto \lambda^{K(q)} \tag{4}$$

where $K(q)$ is the scaling function. The two characterizations $c(\gamma)$, $K(q)$ are related by a Legendre transformation so that there is a unique singularity associated with each moment: $\gamma(q) = K'(q)$.

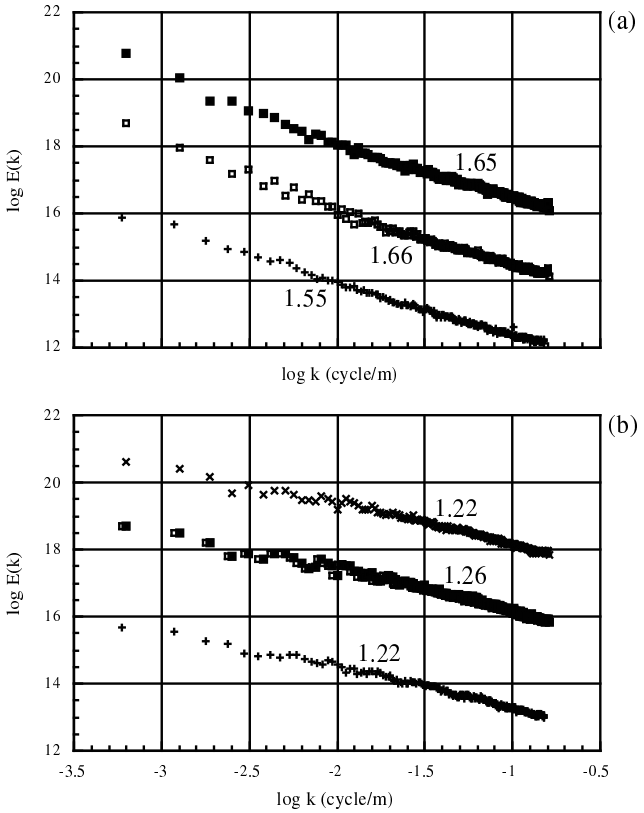

Fig. 2 Spectra from Puu Oo volcanic vent. In **(a)**, spectra from the visible; in **(b)**, spectra from thermal infrared. All spectra were shifted vertically for a better visualization. Corresponding β values are indicated.

Hence, determining either the $K(q)$ or the $c(\gamma)$ functions is a central objective of the present study. Since mathematically, $K(q)$ and $c(\gamma)$ are only constrained to be convex, their specification is equivalent to an infinite number of parameters. Fortunately, due to the existence of stable and attractive multifractal processes, Schertzer and Lovejoy[6] argue that multiplicative cascades can generally be modeled with a limited number of universal parameters defining $K(q)$. Universality implies that laws governing the system are insensitive to many of the details of the model. Universal multifractals have $K(q)$ functions given by:

$$K(q) = \frac{C_1}{\alpha - 1}\left(q^\alpha - q\right), \quad \text{for } 0 \leq \alpha < 1 \text{ and } 1 < \alpha \leq 2 \tag{5}$$

$$K(q) = C_1 q \log(q), \quad \text{for } \alpha = 1. \tag{6}$$

The parameter α describes the degree of multifractality of the field. The maximum $\alpha = 2$ is

the lognormal multifractal (with approximately lognormal statistics) whereas for $\alpha \to 0$, $K(q, \eta)$ becomes linear with q; the monofractal β model. C_1 is the codimension of the mean of the field. The $K(q)$ function defined by α and C_1 are for (scale by scale) conserved multifractal processes: generally, the observed fields are related to these by a fractional integration (power law filter). This introduces a third parameter H which characterizes the degree of non-conservation and will be discussed below. The double trace moment method (DTM) has been elaborated[7] to conveniently estimate the α and C_1. Each intensity of the field at the inner available scale Λ (or at the maximum λ) is raised at the power η then averaged over the intermediate resolution and the qth power of the result is averaged over all available data:

$$\langle (\varepsilon_\Lambda^\eta) \rangle_\lambda^q = \lambda^{K(q,\eta)} \,. \tag{7}$$

Since in general $K(q, \eta) = K(q\eta, 1) - qK(\eta, 1)$, then:

$$K(q, \eta) = \eta^\alpha K(q, 1) \,. \tag{8}$$

Also since $\beta = 1 - K(2) + 2H$, the non-conservation parameter H estimated from α and

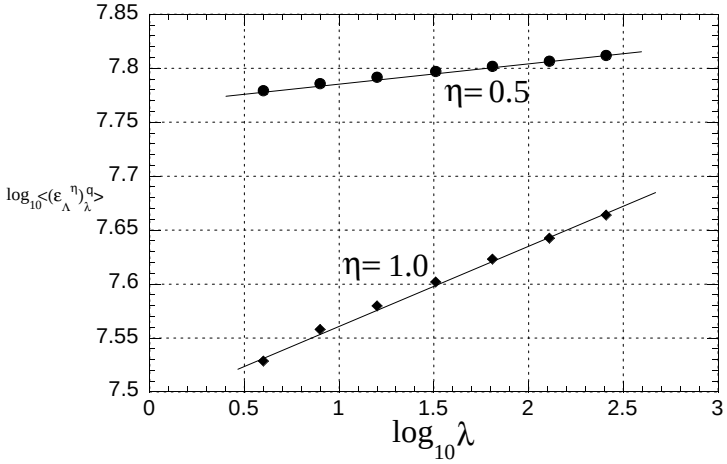

(a)

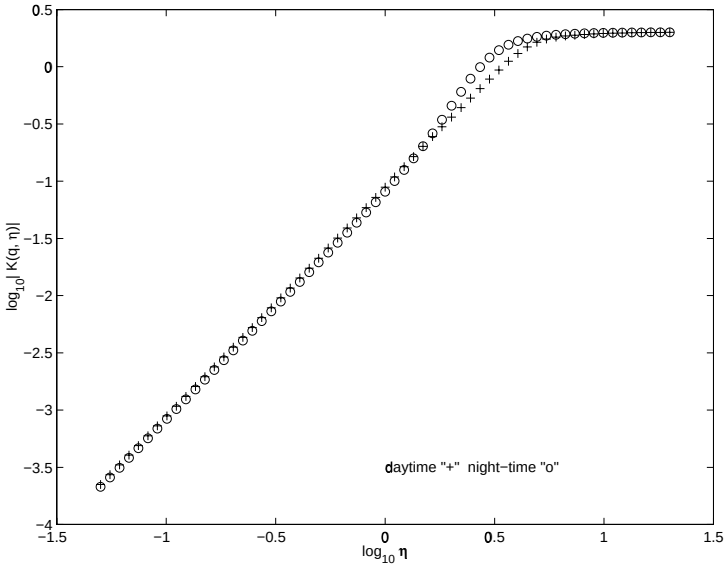

(b)

Fig. 3 In **(a)**, example of multiscaling resulting from double trace moment analysis of an active lava sub-scene from the TIR. In **(b)**, the associated diagram leading to the estimation of α and C_1 for daytime and night-time. Moments for $q = 2.0$ for different values of η.

C_1 and the spectral exponent β can be:

$$H = \frac{\beta - 1}{2} + C_1 \frac{(2^\alpha - 2)}{2(\alpha - 1)}. \qquad (9)$$

It represents the roughness or the smoothness of the field.[21]

We first discuss a necessary technical point, since typical geophysical fields including volcanic visible to thermal fields as well as numerous geophysical fields are generally not conservative, and the DTM only gives accurate results on conservative fields; it is sufficient to take (absolute) derivative of order $> H$ to make them conservative. Because of the low values of dynamic range (8-bit), using a gradient as in Laferrière and Gaonac'h,[5] commonly generates many spurious zero gradients in our analysis, reducing considerably the accuracy of the α-value (which is sensitive to frequent low values). Thus, to reduce the number of zero gradients, we operate a gradient in conjunction with a Fourier-space power law filtering of $k^{(H_f+1)}$ (since the real space gradient is a numerical approximation to derivative order 1, the total order of differentiation is H_f). The accuracy of the C_1 estimates depends somewhat on a specific filter value H_f+1. As long as $H_f \geq H$, we should obtain reasonable estimates of α and C_1. However, in practice the scaling (especially at the small scale) is not as good for some H_f as others (taking the absolute gradients breaks the scaling at the smallest scale). For each sub-scene, we use the filter giving the best (multi-) scaling results to estimate α and C_1. Figure 3 shows two examples of such a multiscaling behavior from our data set.

4. MULTIFRACTAL CHARACTERISTICS OF THE VOLCANIC FEATURES

4.1 Volcanic versus Non-Volcanic Fields

When analyzing remotely sensed data, various geophysical phenomena may be present in one image.

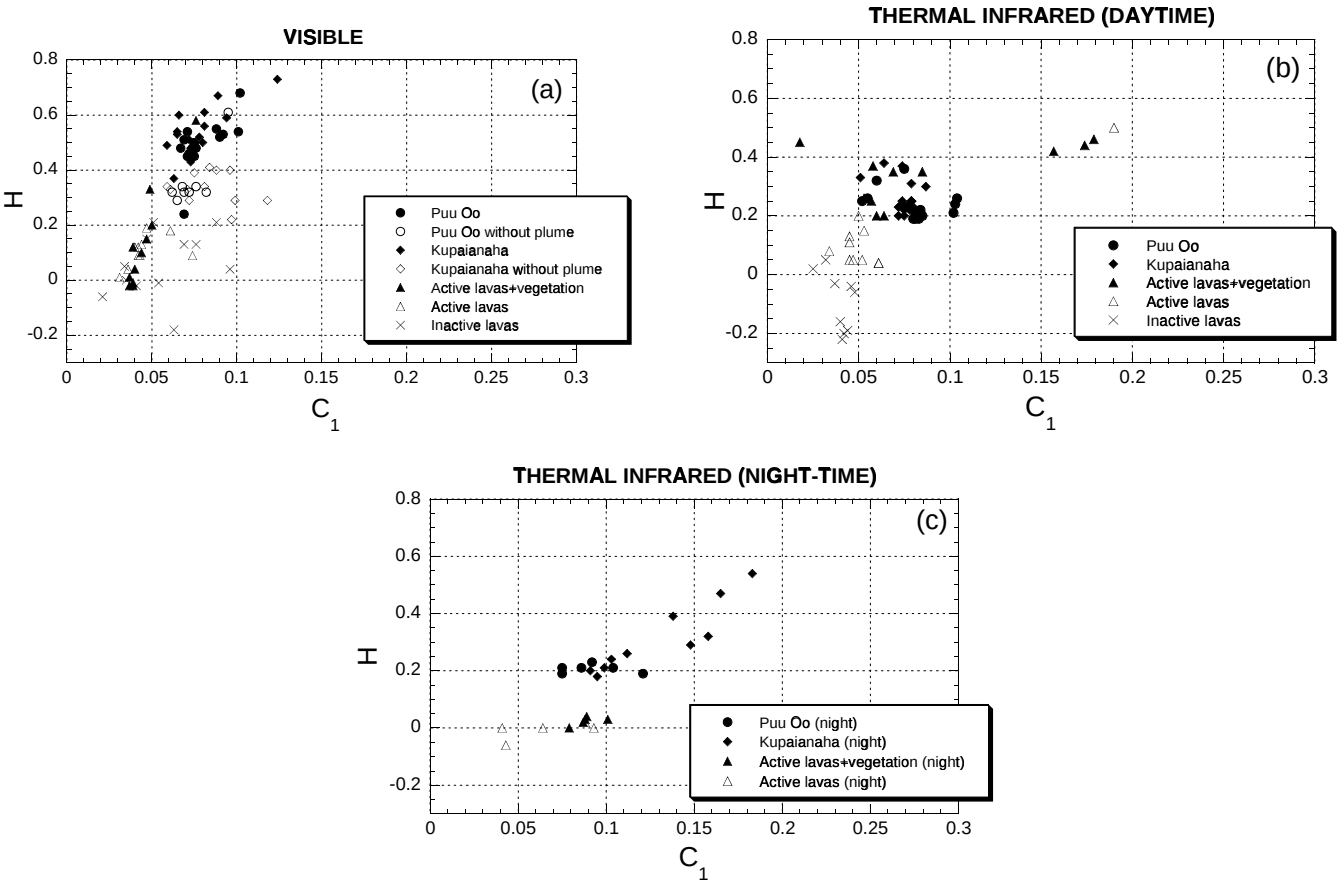

Fig. 4 H versus C_1 diagrams for classes of volcanic structures: **(a)** for the visible; **(b)** and **(c)** for thermal infrared during daytime and night-time measurements, respectively (see text for explanations).

For example, the Puu Oo and Kupaianaha vents were continuously degassing during data acquisition where volcanic gas plumes may have occupied a portion of an image. On Fig. 4(a), there is an evident smoothing effect in the visible due to the presence of these volcanic plumes in the image; it increases the H values to ~ 0.5 while a series of selected images that do not bear any plume is represented by values of $H \sim 0.3$. Similarly, the amount of the vegetation on active lava sub-scenes leads to smoother thermal infrared images [Fig. 4(b)], increasing the H-value from ~ 0.1 to ~ 0.3. The data also show that the vegetation has no detectable effect on the statistics of volcanic fields in the visible. In the TIR, thin plumes are not a serious problem; we therefore did not analyze thermal data for the effect of plumes; instead we considered that these plumes are sufficiently thin to reveal the volcanic surface structures. If present, atmospheric clouds will also perturb the field statistics in both spectral regions. Following these observations, it is therefore convenient to use a revised data set involving as much as possible volcanic fields without cloud/plumes contamination to constrain their statistical properties.

4.2 Statistics in the Visible and Thermal Infrared

Considering the revised data set, we observe differences between volcanic vents and lava flow situated on the flank of the volcano in the visible as well as in the thermal infrared spectra (Fig. 4). Moreover, the values are fairly similar in both wavelengths, suggesting a common origin for the albedo and the thermal field. The obvious mechanism linking both spectral regions is the sun's radiation and the topography: the albedo of the volcanic surface is dependent on the topography via altitude gradients whereas the thermal infrared represents the response via differential solar heating of the surface again sensitive to topographic gradients (surface areas not well exposed to the sun show lower temperatures than surfaces directly oriented to the sun). Furthermore, if the visible reflective properties and TIR heating are dominated by absolute topographic gradients, then the resulting fields have the same α and C_1 but with $H = 0$. This is because if $H < 1$, then the absolute gradient gives us the conserved multifractal with same α and C_1. We propose that the difference between volcanic vents and lava flow is related to differences in the gradient of the topography. Vent areas are dominated by large-scale structures while active and non-active flows show higher variability at fine scales.

When observing the volcanic area during the night [Fig. 4(c)], multifractal estimates demonstrated that H values are generally similar or somewhat smaller than during daytime measurements while C_1 values are generally higher by an amount of ~ 0.03. The cooler night-time background increases the contrast with the surfaces heated by a direct geothermal process. However, Fig. 3(b) shows clearly that the low order, solar heating dominated statistics are hardly changed, so that we obtain only a small decrease (~ 0.1) of the H values from day to night. This diurnal difference has already been mentioned by Gaonac'h et al.[11] who also observed a difference of 0.1 in H values between daytime and night-time helicopter images. The general decrease of solar-source emission creates more isolated thermal features during the night, thus explaining the higher C_1 values. Higher C_1 values characterize a field having more intense spikes that contribute strongly to the mean. This statistical trend is well depicted in daytime sub-scenes [Fig. 4(b)] where a particularly fresh surface lava [corresponding to Fig. 1(f)] present much higher C_1 values. Following this, we propose a general model where low singularities (and hence low q) give statistics that may be related to a solar heating process and where high singularities (high q) are dominated by a geothermal process. In this framework, there is a critical singularity $\gamma(q)$ separating the two phenomenon. In Fig. 3(b), it is apparently at $q\eta \sim 3$ for night-time TIR, but somewhat higher during the day. The critical $\gamma(q)$ may be significantly lower when geothermal activity is high (see the lava breakout in Fig. 1).

4.3 Comparison with Other Geophysical Fields

When comparing our results with those of other geophysical fields (Fig. 5), different conclusions may be drawn. Laferrière and Gaonac'h[5] suggested that the difference in H between the albedo and the topography is due to the fact that the former is related to the gradient of the topography. In the visible albedo fields, the Kilauea volcanic surface exhibits a large range of H values (and to a lesser extent C_1) where the other volcanic studied fields (Etna, Mauna Loa) lie. The selection of sub-images

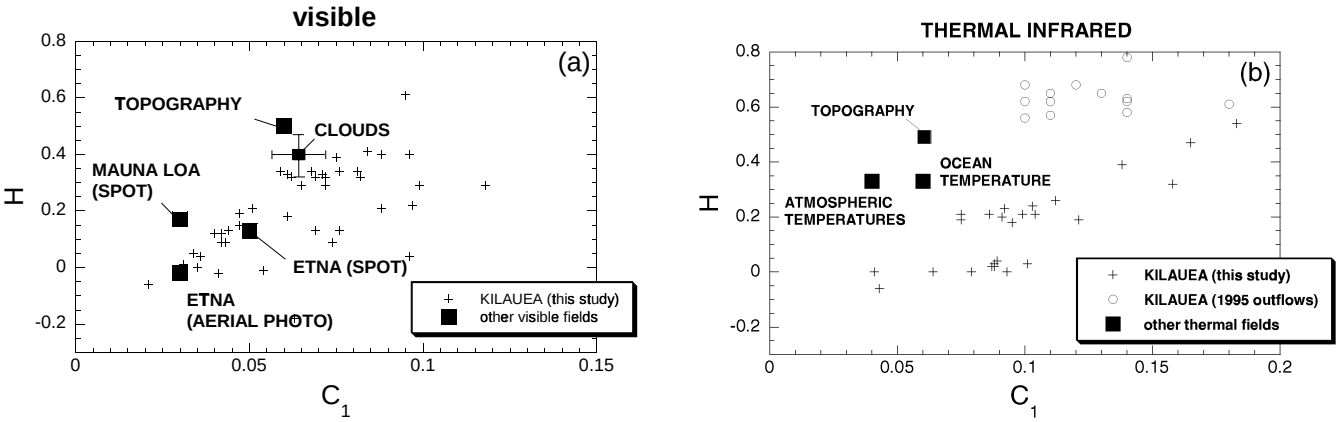

Fig. 5 Comparison of multifractal parameters H and C_1 between Kilauea volcanic field and other visible and thermal infrared geophysical fields.

of a part of a volcano (in our present study) apparently explains the differences observed in H and C_1. When compared to the albedo of clouds,[22,23] we observe that H values of clouds are generally higher than those of volcanic albedo, e.g. $0 < H < 0.7$ within the values region for the images containing volcanic plumes ($H \sim 0.45$ [Fig. 4(a)]); small amount of cloud can either greatly increase or decrease H depending on whether they are diffuse, thin or thick.[23]

When considering the thermal infrared region, their comparison with other geophysical fields reveals that the present Kilauea thermal multifractal statistics fall far from results obtained from a companion paper[11] studying the same Kilauea region for which C_1 values are close to 0.14 and H values close to 0.6. We may explain the difference in the statistics between the two analyzed thermal fields by the dominance of heating of the volcanic surface by the sun in the present study while a dominance of the volcanic heating in Gaonac'h et al.[11] Hence as suggested by these authors, the visible and solar volcanic field presented in this paper is dominated by the gradient of the topography, providing a different H-value ($H \sim 0$ to 0.2), while the geothermal volcanic heating field exhibits a similar H-value compared to the topography ($H \sim 0.5$).

5. CONCLUSION

In this paper, we confirm that volcanically active areas provide highly multiscaling fields over the range of scale of at least 2.5 m to 6 km. The scaling is remarkably well respected and explains the difficulties that traditional approaches have when comparing data at different resolutions. The statistics exhibits a high degree of multifractality ($\alpha \sim 2.0$), a varying $C_1 \sim 0.05$ to 0.12, and a degree of non-conservation of the dynamical process ranging from $H \sim 0.0$ to 0.6. The differences have various causes including the presence of vegetation and volcanic plumes in the volcanic environment. Keeping all these external effects in mind, we are still able to distinguish between vent areas and lava flow flanks of a volcano. We explain this difference by the topography in the visible as well as in the thermal infrared regions where the solar reflection and the thermal emission strongly depend on the local (fine scale) slope of the volcano.

The comparison of the present data with other data sets provides a clue to the importance of the solar versus geothermal volcanic statistics which may be estimated over an area. The H parameter appears to be affected by the dominance of one effect over the other, depending on the observed singularities. The multiscaling of the low solar origin singularities provides an $H \sim 0.0$ to 0.2 similar to the H-value of the volcanic albedo field while the geothermal volcanic field, characterized by higher singularities, is described by an $H \sim 0.6$. The strongly multiscaling behavior of the volcanic fields reveals that we may have to consider the thermal radiative field of a volcano as well as the albedo field through a multiplicative scaling cascade providing small as well as large volcanic structures/anomalies.

Monitoring some volcanic activity in a region may be easily done today by remotely sensed data.

However, when quantitatively analyzing the available data, we need more information than two or three thermal components[3] to objectively characterize the field, particularly its statistics. Hence, the present study reveals that the data provided by the NASA airborne campaign mostly represents the dominance of heating due to the sun. Interpretation of such data is very hazardous as it is based on a very small number of pixels.

More active volcanoes need to be studied around the world, in particular to better constrain the anisotropy versus isotropy of the fields. This is currently in progress. Data acquired at higher resolutions[11] or with a larger dynamic range may better reveal the multiscaling nature of the real active volcanic fields. The implications of this scaling are important in modeling and integrating data in geographic information systems.

ACKNOWLEDGMENTS

This work has been funded by the Fonds pour la Formation de Chercheurs et d'aide à la recherche (FCAR) grants.

REFERENCES

1. C. Oppenheimer and D. A. Rothery, "Infrared Monitoring of Volcanoes by Satellite," *J. Geol. Soc. London* **148**, 563–569 (1991).
2. H. Gaonac'h, J. Vandemeulebrouck, J. Stix and M. Halbwachs, "Thermal Infrared Satellite Measurements of Volcanic Activity at Stromboli and Vulcano," *J. Geophys. Res.* **99**(B5), 9477–9485 (1994).
3. D. A. Rothery, P. W. Francis and C. A. Wood, "Volcano Monitoring Using Short Wavelength Infrared Data from Satellites," *J. Geophys. Res.* **93**, 7993–8008 (1988).
4. H. Gaonac'h, S. Lovejoy and J. Stix, "Scale Invariance of Basaltic Lava Flows and Their Fractal Dimensions," *Geophys. Res. Lett.* **19**(8), 785–788 (1992).
5. A. Laferrière and H. Gaonac'h, "Multifractal Properties of Visible Reflectance Fields from Basaltic Volcanoes," *J. Geophys. Res.* **B104**(3), 5115–5126 (1999).
6. D. Schertzer and S. Lovejoy, "Physical Modeling and Analysis of Rain and Clouds by Anisotropic Scaling of Multiplicative Processes," *J. Geophys. Res.* **92**, 9693–9714 (1987).
7. D. Lavallée, S. Lovejoy, D. Schertzer and P. Ladoy, "Nonlinear Variability of Landscape Topography: Multifractal Analysis and Simulation," in *Fractals in Geography*, eds. L. De Cola and N. Lam (Prentice-Hall, Englewood Cliffs, NJ, 1993), pp. 158–192.
8. Y. Tessier, S. Lovejoy, D. Schertzer, D. Lavallée and B. Kerman, "Universal Multifractal Indices for the Ocean Surface at Far Red Wavelengths," *Geophys. Res. Lett.* **20**, 1167–1170 (1993).
9. S. Lovejoy, D. Schertzer, Y. Tessier and H. Gaonac'h, "Multifractal and Resolution Dependent Remote Sensing Algorithms: The Example of Ocean Colour," *Int. J. Remote Sens.* **22**, 1191–1234 (2001).
10. T. Falco, F. Francis, S. Lovejoy, D. Schertzer, B. Kerman and M. Drinkwater, "Scale Invariance and Universal Multifractals in Sea Ice Synthetic Aperture Radar Reflectivity Fields," *IEEE Trans. Geosci. Remote Sens.* **34**(4), 906–914 (1996).
11. H. Gaonac'h, S. Lovejoy and D. Schertzer, "Multifractal Analysis of Infrared Imagery of Active Thermal Features at Kilauea Volcano," *Int. J. Remote Sens.*, in press (2002).
12. A. Beaulieu and H. Gaonac'h, "Scaling of Differentially Eroded Surfaces in the Drainage Network of the Ethiopian Plateau," *Remote Sens. Env.* **82**, 111–122 (2002).
13. F. Schmitt, S. Lovejoy, D. Schertzer, D. Lavallée and C. Hooge, "First Estimates of Multifractal Indices for Velocity and Temperature Fields," Comptes Rendus de l'Academie des Sciences de Paris, serie II-56 (1992), pp. 749–754.
14. Y. Chigirinskaya, D. Schertzer, S. Lovejoy, A. Lazarev and A. Ordanovich, "Unified Multifractal Atmospheric Dynamics Tested in the Tropics, Part 1: Horizontal Scaling and Self-Organized Critically," *Nonlinear Process. Geophys.* **1**, 105 (1994).
15. D. L. Turcotte, "A Fractal Interpretation of Topograpy and Geoid Spectra on the Earth, Moon, Venus and Mars," *J. Geophys. Res.* **92**, 597-601 (1987).
16. F. Schmitt, D. Schertzer and S. Lovejoy, "Turbulent Fluctuation in Financial Markets: A Multifractal Approach," in *Chaos Fractal Models*, eds. F. M. Guindani and G. Salvadori (Italian University Press, 1998).
17. D. Marsan and C. J. Bean, "Multiscaling Nature of Sonic Velocities and Lithology in the Upper Crystalline Crust: Evidence from the KTB Main Borehole," *Geophys. Res. Lett.* **26**, 275–278 (1999).
18. E. A. Novikov and R. Stewart, "Intermittency of Turbulence and Spectrum of Fluctuations in Energy Dissipation," *Izv. Akad. Nauk. SSSR. Ser. Geofiz.* **3**, 408–412 (1964).
19. A. M. Yaglom, "The Influence on the Fluctuation in Energy Dissipation of the Shape of Turbulent Characteristics in the Inertial Interval," *Sov. Phys. Dolk.* **2**, 26 (1966).
20. B. B. Mandelbrot, "Intermittent Turbulence in Self-Similar Cascades: Divergence of High Moments

and Dimension of the Carrier," *J. Fluid. Mech.* **62** 331–350 (1974).
21. S. Pecknold, S. Lovejoy, D. Schertzer and C. Hooge, "Multifractals and Resolution Dependence of Remotely Sensed Data: GSI to GIS," in *Scale in Remote Sensing and GIS*, eds. D. A. Quattrochi and M. F. Goodchild (CRC Lewis Publishers, Boca Raton, FL, 1997), pp. 361–394.
22. J. D, Stanway, M. Sc. Thesis, Department of Physics, McGill University, Canada.
23. D. Sachs, S. Lovejoy and D. Schertzer, "The Multifractal Scaling of Cloud Radiances from 1 m to 1 km," *Fractals*, this issue.